Noise generation by turbulence interacting with an aerofoil with a serrated leading edge

James Mathews* and N Peake†

University of Cambridge, Cambridge, CB3 0WA, UK

This study considers the interaction of turbulence with a serrated leading edge. We investigate the noise produced by an aerofoil moving through a turbulent perturbation to uniform flow by considering the scattered pressure from the leading edge. To do this we develop an analytical model which allows us to consider both deterministic eddies and turbulence. We show that it is possible to reduce the noise by using a serrated leading edge compared with a straight edge, but the optimal noise-reducing choice of serration is hard to predict.

Nomenclature

$\boldsymbol{A}$	Amplitudes of eddy $\boldsymbol{\Phi}$
$\boldsymbol{B}$	Gaussian stengths of eddy $\boldsymbol{\Phi}$
$\boldsymbol{C}$	Amplitudes of eddy $\boldsymbol{\Psi}$
$\boldsymbol{D}$	Gaussian strengths of eddy $\boldsymbol{\Psi}$
G^f	Green's function for an aerofoil defined by $x > f(z), y = 0$
$G^{f,\alpha}$	Green's function for an aerofoil at angle of attack α and leading edge serration $f(z)$
P_f	Power of the scattered pressure
R	Eddy radius, dependent on source position of the eddy
U	Base flow velocity
c_0	Speed of sound
$\boldsymbol{e}_i$	Unit vector in i-th direction
f	Serration function
k_0	Wavenumber, $k_0 = \omega/c_0$
p	Pressure perturbation
p_0	Base flow pressure
p_i	Incident pressure
p_s	Scattered pressure
(r, θ, z)	Cylindrical coordinates in x-y plane, centred at $(0, 0)$
(r^*, θ^*, z^*)	Modified cylindrical coordinates in x-y plane, centred at $(f(z), 0)$
$(r^\star, \theta^\star, z^\star)$	Modified cylindrical coordinates in x-y plane for an angle of attack α, centred at $(f(z)\cos\alpha, -f(z)\sin\alpha)$
t	Time
$\boldsymbol{u}$	Perturbation velocity of the form (u, v, w)
w	Frequency of the serration $f(z) = A\sin(wz)$
$\boldsymbol{x}$	Cartesian coordinates of the position, $\boldsymbol{x} = (x, y, z)$
$\boldsymbol{x}_0$	Cartesian coordinates of the source, $\boldsymbol{x}_0 = (x_0, y_0, z_0)$
$\boldsymbol{x}_e$	Source position the eddy, $\boldsymbol{x}_e = (x_e, y_e, z_e)$
x_1	Frequent change of variables given by $x_1 = x_0 + f(z_0)$

*Ph.D student, Department of Applied Mathematics and Theoretical Physics (DAMTP), jrm214@cam.ac.uk. Student member.

†Professor, Department of Applied Mathematics and Theoretical Physics (DAMTP), np100@cam.ac.uk. Senior member.

$\boldsymbol{z}_s$	Centre of modified cylindrical coordinates for arbitrary z_0, given by $(f(z), 0, z_0)$
$\boldsymbol{\Phi}$	Eddy
$\boldsymbol{\Psi}$	Eddy
α	Angle of attack
β_{ij}	Product of amplitudes and Gaussian strengths in i and j direction, for a single eddy $\beta_{ij} = A_i B_i A_j B_j$
γ_{ij}	Sum of Gaussian strengths in i and j direction, for a single eddy $\gamma_{ij} = B_i + B_j$
$\boldsymbol{\varepsilon}$	Distance between two sources given by $\boldsymbol{\varepsilon} = (\varepsilon_x, \varepsilon_y, \varepsilon_z) = \boldsymbol{x}_e^{\Phi} - \boldsymbol{x}_e^{\Psi}$
λ	Angle of the serration at the origin
ρ	Density perturbation
ρ_0	Base flow density
ω	Frequency
$\mathbb{P}$	Ratio between power of a fixed serration and straight serration
$\mathcal{P}_i$	Fourier transform of incident pressure
$\mathcal{P}_s$	Fourier transform of scattered pressure

I. Introduction

We are interested in trying to find the noise generated by an aerofoil with a serrated leading edge when interacting with turbulence. This is a very relevant problem, because recent experiments and CFD calculations by Haeri et al[1] and Narayana et al[2] respectively have shown that leading-edge serrations can significantly reduce noise. Following on from Howe's[3] work on trailing-edge serrations, we will consider a scattering problem, where the incident pressure (the pressure generated without the presence of the aerofoil) is scattered by the edge of the aerofoil. We will show that the noise generated will depend on two factors, the incident pressure and the Green's function of the aerofoil. We will see that the Green's function will depend on the geometry of the aerofoil, whilst the incident pressure will be determined by using the Navier–Stokes equations in a model for turbulence.

(a) Humpback whale flipper (b) Whale inspired blade

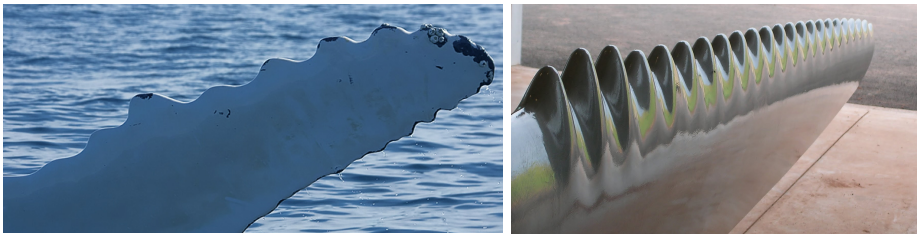

Figure 1: A humpback whale flipper and a whale inspired blade produced by WhalePower. Pictures taken from `http://tinyurl.com/flipperwhale` and `http://tinyurl.com/WhalePowerblade`.

The inspiration for looking at serrations comes from nature, more precisely a flipper of a humpback whale. We can clearly see in Figure 1a that the whale has both a leading- and a trailing-edge serration on its flipper, and also that they are different. A company called WhalePower[4] has already began to use leading-edge serrations (or as they call it, the "tubercle effect") to develop wind turbines and improve the efficiency of fans. An example of an early prototype they made is shown in Figure 1b.

We will begin our analysis by looking at the Green's function for a half plane, and then add serrations to the leading edge. We will use a model of turbulence driven by a number of eddies by Haeri et al,[1] firstly considering one eddy and investigating the effect of the eddy parameters on the reduction of the noise from a leading-edge serration. We will then consider the effect of multiple eddies, and show they interact with each other in a nonlinear way, and further consider random parameters for the eddies. Finally, we will consider an aerofoil at a small angle of attack.

II. The Green's function

We wish to calculate the Green's function for the aerofoil in Figure 2. Although we can compute the Green's function numerically, we wish to compute an approximate analytic Green's function which will both increase the speed of computations and allow an insight to the dynamics involved.

A. Geometry of the aerofoil

We approximate the aerofoil as a thin plate, so it is modelled as a rigid plane S with $y = \pm 0$ and defined by $x > f(z)$ for some function f, as shown in Figure 2. If there are no serrations then $f(z) = 0$ and

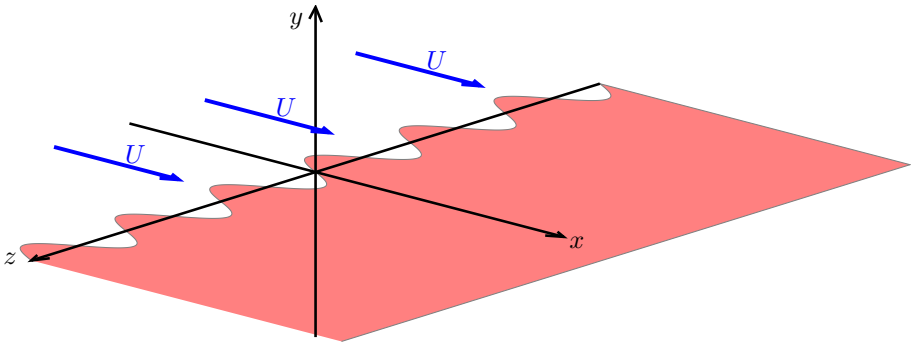

Figure 2: Geometry of the aerofoil with serrations $x = f(z)$.

S is a half plane. We assume the mean velocity flow is given by $(U, 0, 0)$. Whilst our assumptions of infinite chord and infinite wingspan are not realistic they are needed to make some initial progress on the Green's function.

B. Howe's approach

In Howe's[3] approach we can split the pressure into the incident pressure p_i and scattered pressure p_s, with $p(\boldsymbol{x}, t) = p_i(\boldsymbol{x}, t) + p_s(\boldsymbol{x}, t)$. We further define $\mathcal{P}_i(\boldsymbol{x}, \omega)$ and $\mathcal{P}_s(\boldsymbol{x}, \omega)$ to be the inverse Fourier transforms of p_i and p_s (with time dependence $\exp(-i\omega t)$), then in high Reynolds number, low Mach number flow we have

$$(\Delta + k_0^2)\mathcal{P}_s = 0, \tag{1}$$

for wavenumber $k_0 = \omega/c_0$, since we can ignore convection and scattering by the flow. The inverse Fourier transform allows us to convert from the wave equation to the Helmholtz equation. We also have the boundary condition

$$\frac{\partial \mathcal{P}_i}{\partial y} + \frac{\partial \mathcal{P}_s}{\partial y} = 0, \tag{2}$$

on the aerofoil. This boundary condition stems from Fourier transforming the full Navier–Stokes equation in uniform flow, given by

$$\frac{\partial p}{\partial y} = \rho \left[\frac{\partial v}{\partial t} + \nabla v \cdot ((U, 0, 0) + (u, v, w)) \right] \tag{3}$$

$$= \rho \left[\left(\frac{\partial}{\partial t} + U \frac{\partial}{\partial x} \right) v + u \frac{\partial v}{\partial x} + v \frac{\partial v}{\partial y} + w \frac{\partial v}{\partial z} \right] = 0, \tag{4}$$

where the velocity is $\boldsymbol{u} = (U, 0, 0) + (u, v, w)$ and we have $v = 0$ on the aerofoil. Using the Kirchhoff integral formula (essentially Green's second identity) and the boundary conditions, we calculate[5] the scattered pressure is given by

$$\mathcal{P}_s^f(\boldsymbol{x}, t) = -\int_{-\infty}^{\infty} \int_0^{\infty} \frac{\partial \mathcal{P}_i}{\partial y}(x_1 + f(z_0), 0, z_0, \omega)[G^f(\boldsymbol{x}, (x_1 + f(z_0), z_0); \omega)] \mathrm{d}x_1 \mathrm{d}z_0, \tag{5}$$

where $[G^f]$ is the the jump of the Green's function for Helmholtz's equation over the aerofoil. We have performed a change of variables $x_1 = x_0 + f(z)$ to make the integration region simpler.

C. Serrated coordinates

We introduce the coordinates (r^*, θ^*, z^*) defined by

$$(x, y, z) = (f(z^*) - r^* \cos\theta^*, -r^* \sin\theta^*, z^*), \tag{6}$$

which are modified cylindrical coordinates in the x-y plane centred at $(f(z^*), 0)$. In the case of $f(z) = 0$ they are just cylindrical coordinates. We define the angle θ such that $\theta^* = \pi$ above the aerofoil, and $\theta^* = -\pi$ below the aerofoil, which gives the minus sign in the definition of the coordinates. Since we have $z = z^*$ we will just use the former for clarity.

D. Green's function for serrated leading edge

With a straight leading edge ($f(z) = 0$) and in the far field with $r \gg r_0$ the Green's function of Helmholtz's equation is given by[6]

$$G^0(r, \theta, z|r_0, \theta_0, z_0) = -\frac{1}{4\pi} \sum_{n=0} a_n \cos\nu(\theta + \pi) \cos\nu(\theta_0 + \pi) J_\nu(k_0 r_0 \sin\chi) \frac{e^{ik_0|\boldsymbol{x} - \boldsymbol{e}_z z_0|}}{|\boldsymbol{x} - \boldsymbol{e}_z z_0|} e^{-i\pi\nu/2}, \tag{7}$$

where $\nu = n/2$, $a_0 = 1$, $a_n = 2$ and $\tan\chi = r/(z - z_0)$. This can also be derived following Duffy,[7] where we extend the result from a circular sector in two dimensions to three dimensions and let the angle of the sector tend to zero. We require that the Green's function is finite at the trailing edge of the aerofoil, to ensure that the unsteady Kutta condition is satisfied.[3] Following Howe[6] and assuming that $k_0 r_0$ is small, we can just consider the first two terms of the sum, G_0^0 and G_1^0. However, we have $[G_0^0] = 0$ and hence we can approximate the jump in the Green's function as

$$[G^0(\boldsymbol{x}, (x_1, z_0); \omega)] \approx [G_1] = -\frac{\sqrt{2}}{\pi\sqrt{\pi i}} \frac{\sqrt{k_0}\sqrt{r}\sin(\theta/2)}{|\boldsymbol{x} - \boldsymbol{e}_z z_0|^{3/2}} e^{ik_0|\boldsymbol{x} - \boldsymbol{e}_z z_0|} |x_1|^{1/2}. \tag{8}$$

When we find the Green's function for serrations, we get a very similar result

$$[G^f(\boldsymbol{x}, (x_1 + f(z_0), z_0); \omega)] \approx -\frac{\sqrt{2}}{\pi\sqrt{\pi i}} \frac{\sqrt{k_0}\sqrt{r^*}\sin(\theta^*/2)}{|\boldsymbol{x} - \boldsymbol{z}_s|^{3/2}} e^{ik_0|\boldsymbol{x} - \boldsymbol{z}_s|} |x_1|^{1/2}, \tag{9}$$

where $\boldsymbol{z}_s = (f(z), 0, z_0)$. Note that the Green's function formula in Eq. (7) is exact for a straight edge. To calculate the Green's function for a serrated edge we needed to assume that $|f'(z)|$ is small, which is equivalent to the slender body approximation.[3] Shallow serrations are needed for two reasons. Firstly, when we consider Helmholtz's equation in the new serrated coordinates (by performing a change of variables) we are able to discard all the extra terms and thus we have

$$\frac{\partial^2}{\partial x^2} + \frac{\partial^2}{\partial y^2} + \frac{\partial^2}{\partial z^2} + k_0^2 \approx \frac{\partial^2}{\partial r^{*2}} + \frac{1}{r^*}\frac{\partial}{\partial r^*} + \frac{1}{r^{*2}}\frac{\partial^2}{\partial \theta^{*2}} + \frac{\partial^2}{\partial z^2} + k_0^2. \tag{10}$$

Secondly, we need the serrations to be shallow so that the normal of the aerofoil lies approximately in a plane of fixed z, this then allows us to move from two dimensions in x-y to a third dimension in z.

Howe[3] goes on to argue that the slender body approximation can be extended for non shallow serrations, and provides an upper bound on the pressure, although that relies on his form on the incident pressure, which is different.

We now have an approximate analytic Green's function that can be used for any model of turbulence, and the rest of the paper considers one particular model of turbulence and its effect on the scattered pressure when we vary the leading-edge serrations.

III. Modelling the turbulence

In Haeri et al[1] the turbulence is modelled as a sum of eddies, where each eddy has different parameters and can take difference "shapes". The turbulent velocity is given by a vorticity perturbation, so we have

$$\boldsymbol{U}(\boldsymbol{x}, t) = (U, 0, 0) \text{ and } \boldsymbol{u}(\boldsymbol{x}, t) = \nabla \times \boldsymbol{\Phi}(\boldsymbol{x}, t), \tag{11}$$

where $\boldsymbol{\Phi}$ is the vorticity. It is defined in Haeri et al[1] as a sum of eddies, given by

$$\boldsymbol{\Phi}(\boldsymbol{x},t) = A\sum_{i=1}^{N_e}\left(\Phi_{x,i}(\boldsymbol{x},t)\boldsymbol{e}_x + \Phi_{y,i}(\boldsymbol{x},t)\boldsymbol{e}_y + \Phi_{z,i}(\boldsymbol{x},t)\boldsymbol{e}_z\right), \tag{12}$$

where $\Phi_{\xi,i}$ are shape functions with Gaussian or Mexican hat profiles as functions of

$$R_i(\boldsymbol{x},t) = (x - x_{0,i} - Ut)^2 + (y - y_{0,i})^2 + (z - z_{0,i})^2, \tag{13}$$

where $(x_{0,i}, y_{0,i}, z_{0,i})$ denotes where the i-th eddy first appears. For now we are free to choose the parameters, but later we will choose the numerous parameters of the eddy stochastically. To calculate the pressure we use the full Navier–Stokes equation, for which the momentum equation can be written as

$$\rho_0\left(\frac{\partial \boldsymbol{u}}{\partial t} + \boldsymbol{U}\cdot\nabla\boldsymbol{u}\right) + \nabla p = -\rho_0\boldsymbol{u}\cdot\nabla\boldsymbol{u} - \rho\left(\frac{\partial \boldsymbol{u}}{\partial t} + \boldsymbol{U}\cdot\nabla\boldsymbol{u} + \boldsymbol{u}\cdot\nabla\boldsymbol{u}\right), \tag{14}$$

where p and ρ are pressure and density perturbations to the constant pressure p_0 and constant density ρ_0. We note that since Φ is a function of R_i then we necessarily have

$$\frac{\partial \boldsymbol{u}}{\partial t} + \boldsymbol{U}\cdot\nabla\boldsymbol{u} = \boldsymbol{0}. \tag{15}$$

Hence to leading order we have $\partial p/\partial y = 0$ but to second order we have

$$\frac{\partial p}{\partial y} = -\rho_0\boldsymbol{u}\cdot\nabla v. \tag{16}$$

This nonlinear form of the pressure will lead to difficulties when we consider more than one eddy, since in particular each eddy will interact with every other eddy.

A. A single eddy

We firstly consider a single eddy, so we assume $\boldsymbol{\Phi}$ is of the form

$$\boldsymbol{\Phi}(\boldsymbol{x},t) = A_1e^{-B_1R}\boldsymbol{e}_x + A_2e^{-B_2R}\boldsymbol{e}_y + A_3e^{-B_3R}\boldsymbol{e}_z, \tag{17}$$

with R given by Eq. (13). We have also assumed the shape function is given by a Gaussian profile. Note that since the total incident pressure p_i is given by $p_i = p + p_0$, with p_0 constant, then we have $\partial p_i/\partial y = \partial p/\partial y$. After inserting $\boldsymbol{\Phi}$ into Eq. (16) and performing a lengthy calculation, we find that

$$\frac{\partial p_i}{\partial y}(x,0,z,t) = -4\rho_0[(x - x_e - Ut)\beta_{12}e^{-\gamma_{12}R} + \beta_{23}(z - z_e)e^{-\gamma_{23}R} + \beta_{11}e^{-\gamma_{11}R} + \beta_{33}y_ee^{-\gamma_{33}R}], \tag{18}$$

where $\beta_{ij} = A_iA_jB_iB_j$ and $\gamma_{ij} = B_i + B_j$. We can write $e^{-\gamma R}$ as $e^{-\gamma U^2(t-(x-x_e)/U)^2}e^{-\gamma(z-z_e)^2}e^{-\gamma y_e^2}$, and then using the relations

$$\int_{\mathbb{R}} e^{-\gamma(t-\delta)^2}e^{i\omega t}\mathrm{d}t = e^{i\omega\delta}e^{-\omega^2/4\gamma}\sqrt{\frac{\pi}{\gamma}} \text{ and } \int_{\mathbb{R}} te^{-\gamma(t-\delta)^2}e^{i\omega t}\mathrm{d}t = e^{i\omega\delta}e^{-\omega^2/4\gamma}\sqrt{\frac{\pi}{\gamma}}\left[\delta + \frac{i\omega}{2\gamma}\right], \tag{19}$$

we can calculate the inverse Fourier transform as

$$\frac{\partial \mathcal{P}_i}{\partial y}(x,0,z,\omega) = \frac{-2\rho_0}{U\sqrt{\pi}}\left[\beta_{23}(z - z_e)\mathbb{E}_{\gamma_{23}}(\boldsymbol{x},\omega) + \beta_{11}y_e\mathbb{E}_{\gamma_{11}}(\boldsymbol{x},\omega) + \beta_{33}y_e\mathbb{E}_{\gamma_{33}}(\boldsymbol{x},\omega) - \frac{i\omega}{2\gamma_{12}U}\beta_{12}\mathbb{E}_{\gamma_{12}}(\boldsymbol{x},\omega)\right], \tag{20}$$

where $\mathbb{E}_\gamma$ is the product of exponential terms;

$$\mathbb{E}_\gamma(\boldsymbol{x},\omega) = \frac{1}{\sqrt{\gamma}}e^{-\gamma(z-z_e)^2}e^{-\gamma y_e^2}e^{i\omega(x-x_e)/U}e^{-\omega^2/(4\gamma U^2)}. \tag{21}$$

Thus, we have calculated the incident pressure analytically (or more precisely, the derivative of the inverse Fourier transform of the incident pressure) and we can insert this and the Green's function defined in Eq. (9) into the Kirchhoff formula in Eq. (5) to calculate the scattered pressure. This is given by

$$\mathcal{P}_s^f(\boldsymbol{x},\omega) = A\sqrt{r^*}\sin(\theta^*/2)\int_{-\infty}^{\infty}\frac{e^{ik_0|\boldsymbol{x}-\boldsymbol{z}_s|}}{|\boldsymbol{x}-\boldsymbol{z}_s|^{3/2}}Q(z_0,\omega)\mathrm{d}z_0, \tag{22}$$

where

$$A = -\frac{2\rho_0\sqrt{2}}{\pi^2\sqrt{\pi i c_0}}, \tag{23}$$

and

$$Q(z_0,\omega) = -\frac{\pi\omega^{1/2}}{2\rho_0}\int_0^{\infty} x_1^{1/2}\frac{\partial\mathcal{P}_0}{\partial y}(x_1+f(z_0),0,z_0,\omega)\mathrm{d}x_1. \tag{24}$$

The constant A can be ignored since it is independent of the serration and eddy, and we can calculate Q

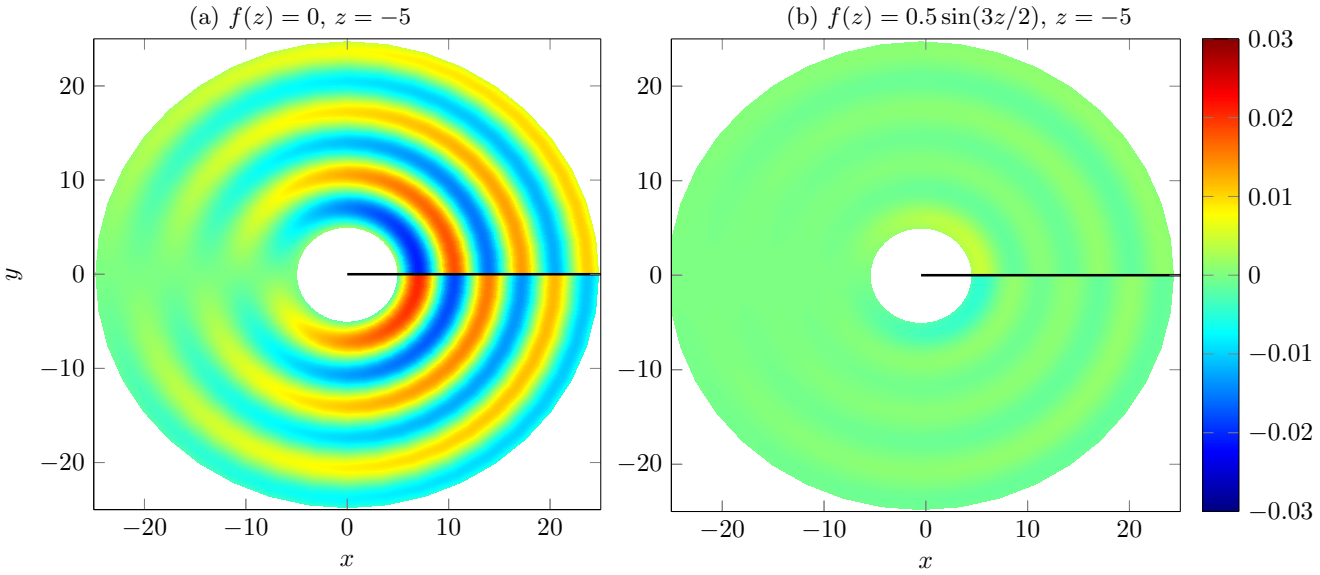

Figure 3: Plot of real part of $\mathcal{P}_s^f(\boldsymbol{x},\omega)/A$ for a non serrated and serrated edge at fixed $z = -5$. We have set $\omega = 1$, $c = 1$, $U = 0.5$, $k_0 = 1$ with eddy parameters $\boldsymbol{A} = (1,2,1)$, $\boldsymbol{B} = (1,1,2)$ and $\boldsymbol{x}_e = (0,0,0)$.

analytically, although we need to use the theory of generalised integrals[8] to evaluate integrals such as

$$\int_0^{\infty} x_1^{1/2}e^{i\omega x_1/U}\mathrm{d}x_1 = e^{3\pi i/4}\frac{\sqrt{\pi}}{2}\frac{U^{3/2}}{\omega^{3/2}}, \tag{25}$$

for positive ω. These integrals are calculated by multiplying the integrand by $e^{-\varepsilon x}$ and calculating the limit as $\varepsilon \to 0$. If we define

$$Q^*_{\beta,\gamma}(z_0,\omega) := \frac{U^{1/2}}{2\omega}\frac{\beta\pi e^{3\pi i/4}}{\sqrt{\gamma}}e^{-\gamma y_e^2}e^{-\omega^2/(4\gamma U^2)}e^{-i\omega x_e/U}e^{-\gamma(z_0-z_e)^2}e^{i\omega f(z_0)/U}, \tag{26}$$

we can use Eq. (25) to conclude that

$$Q(z_0,\omega) = (z_0-z_e)Q^*_{\beta_{23},\gamma_{23}}(z_0,\omega) + y_eQ^*_{\beta_{11},\gamma_{11}}(z_0,\omega) + y_eQ^*_{\beta_{33},\gamma_{33}}(z_0,\omega) - \frac{i\omega}{2\gamma_{12}U}Q^*_{\beta_{12},\gamma_{12}}(z_0,\omega). \tag{27}$$

Thus, we can calculate the inverse Fourier transform of scattered pressure almost analytically, and we are left with the integration with respect to z_0, which is given by integrals of the form

$$\int_{-\infty}^{\infty}\exp\left(ik_0\left[r^{*2}+(z-z_0)^2\right]^{1/2}\right)\left[r^{*2}+(z-z_0)^2\right]^{-3/4}e^{-\gamma(z_0-z_e)^2}e^{i\omega f(z_0)/U}\mathrm{d}z_0. \tag{28}$$

These integrals should be done numerically, but if we want a crude analytical approximation we should consider the integral

$$\exp\left(ik_0\left[r^{*2}+(z-z_e)^2\right]^{1/2}\right)\left[r^{*2}+(z-z_e)^2\right]^{-3/4}\int_{-\infty}^{\infty}e^{-\gamma(z_0-z_e)^2}e^{i\omega\left[f(z_e)+(z_0-z_e)f'(z_e)\right]/U}\mathrm{d}z_0, \qquad (29)$$

which can be integrated exactly using Eq. (19). Since the serrations already had to be shallow for the calculation of the Green's function, expanding $f(z_0)$ about z_e will be a good approximation. Note that this approximation will only be valid if γ is not small. We will briefly consider this analytical approximation in Figure 6, but for the rest of the study the z_0 integration is computed numerically. In the future we could study different analytical approximations of these integral.

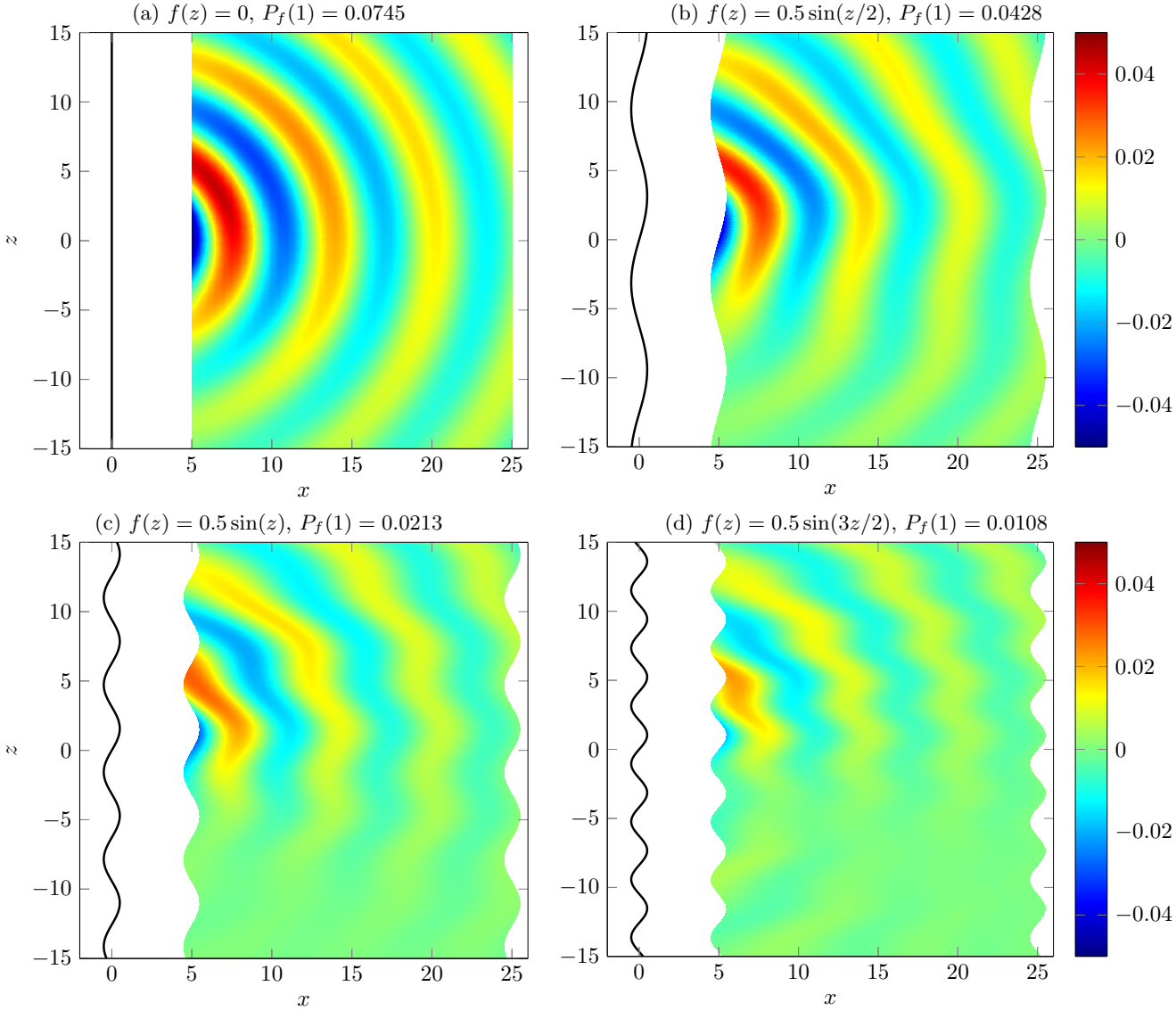

Figure 4: Plot of real part of $\mathcal{P}_s^f(\boldsymbol{x},\omega)/A$ for a non serrated and serrated edge and fixed $\theta^* = \pi$. We have set $\omega = 1$, $c = 1$, $U = 0.5$, $k_0 = 1$ with eddy parameters $\boldsymbol{A} = (1,2,1)$, $\boldsymbol{B} = (1,1,2)$ and $\boldsymbol{x}_e = (0,0,0)$. To get the results for other values of θ^* we multiply the results by $\sin(\theta^*/2)$.

In Figures 3 and 4 we show some results of our calculations. We have calculated the integration with respect to z_0 with a standard numerical solver and plotted $\mathcal{P}_s$ for an eddy with source of $x_e = (0,0,0)$. The other parameters we used are mentioned in the figure. Since the Green's function approximation by Howe (Eq. (9)) is only valid in the far field[3] we have only plotted the pressure for $r > 5$, and in this case up to $r = 25$. We have plotted different views in the figures; a slice in x-y space for Figure 3 and a projection onto the aerofoil in x-z space in Figure 4. In both figures the results are quite remarkable and look very

hopeful. We can see that moving from a straight edge to a serration function of the form $f(z) = 0.5\sin(3z/2)$ reduces the scattered pressure considerably, and furthermore as we increase the frequency of the serration from 0 to 3/2 the noise reduces in a consistent form. Note that the maximum serration we have looked at, $f(z) = 0.5\sin(3z/2)$ has $|f'(z)| < 3/4$ and hence can still be considered shallow and our approximate Green's function still valid. We would expect there to be an optimum serration, at which the scattered pressure is minimised, and after which the scattered pressure begins to increases. However, the restriction of having to use a shallow serration means we may not be able to reach it, which is the case with the current eddy parameters. We will consider a wider range of parameters for the eddy in the next section which will enable us to pass a true judgement on the results.

To get a global measure of the effect of serrations we introduce the power of the scattered pressure, given by

$$P_f(\omega) = \iiint |\mathcal{P}_s^f(r^*, \theta^*, z, \omega)|^2 r^* \mathrm{d}\theta^* \mathrm{d}r^* \mathrm{d}z. \tag{30}$$

We will do the r integration over the region shown in the pictures, so $5 < r < 25$, while the θ integration is easily done analytically between 0 and π and can be ignored from now on. In theory, the z integration will be the average over one wavelength, so if $f(z) = \sin(\lambda z)$ then we would calculate

$$P_f(\omega) = \frac{\lambda}{\pi} \int_{-\pi/2\lambda}^{\pi/2\lambda} \int_5^{25} |\mathcal{P}_s^f(r^*, \pi, z, \omega)|^2 r^* \mathrm{d}r^* \mathrm{d}z. \tag{31}$$

However, when we calculate the limit of this for a straight leading edge we run into numerical problems, so we instead choose to integrate over a fixed region of z space given by $[-6\pi, 6\pi]$:

$$P_f(\omega) = \frac{1}{12\pi} \int_{-6\pi}^{6\pi} \int_5^{25} |\mathcal{P}_s^f(r^*, \pi, z, \omega)|^2 r^* \mathrm{d}r^* \mathrm{d}z. \tag{32}$$

We chose this range since it should mean that most of the serrations wavelengths we choose will exactly divide it. We have computed the power of the serrations in Figure 4 and we can see a noticeable reduction as we increase the frequency of the serration. We will use P_f as a measure of the noisiness of the serrations, a lower value of P_f means the aerofoil is quieter.

B. Noisy serrations

BEFORE we investigate the role of parameters in more detail we look at whether the serrations always reduce the noise or whether they can actually increase the noise compared with a straight leading edge. What happens depends on the angle of the eddy in the x-z plane (which can be calculated from A_1 and A_3) and how this compares to the serration at z_0. In Figure 5 we plot a straight edge and serrated edges of the form $\pm 0.5\sin(z)$. If the eddy and the serration are nearly parallel, as seen in Figure 5c then we will reduce the scattered pressure considerably. However, if the eddy and the serration are nearly perpendicular then we will increase the noise compared with a straight leading edge, as seen in Figure 5a.

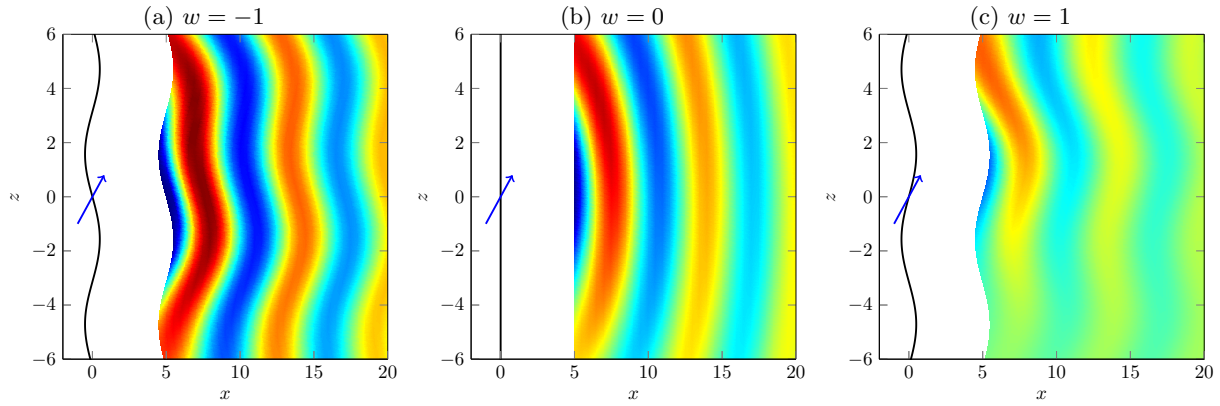

Figure 5: Effect of changing the serration of the form $f(z) = 0.5\sin(wz)$, it is clear we want the angle of the eddy (blue) to be as close to the serration as possible to reduce noise. The only relevant parameters are $A_1 = 1$, $A_3 = 1$ and $z_0 = 0$.

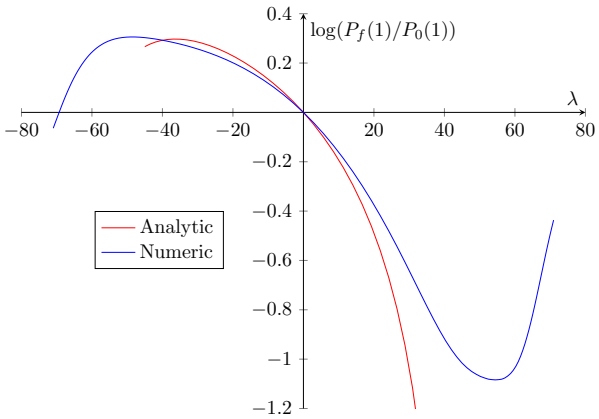

Figure 6: Plot of $\log(P_f(1)/P_0(1))$, against serration angle λ. The eddy parameters are the same as in Figure 5, which are $\boldsymbol{A} = (1, 1, 1)$, $\boldsymbol{B} = (1, 1, 2)$ and $\boldsymbol{x}_e = (-2, 0, 0)$. We have also plotted in red the same result but where we have performing the z_0 integration analytically using the result in Eq. (29).

Note that if a serration $x = f(z)$ reduces the scattered pressure compared with a straight edge, then the serration $x = -f(z)$ will increase it. Thus, we either have the scattered pressure constant across all serrations or we can find at least one serration where we reduce the scattered pressure for a serrated leading edge compared with a straight leading edge. In Figure 6 we look at the same parameters of the eddy. We plot the power of the scattered pressure against the angle λ of the serration at the origin, which is given by $\lambda = \arctan(0.5w)$ for a leading-edge serration of the form $f(z) = 0.5\sin(wz)$. Ignoring the fact that we require $w < 2$ for our serrations to be shallow, we see that the optimum angle of the serration for the eddy with $A_1 = 1$ and $A_3 = 1$ is around $54°$, while the worst serration is at around $-48°$. We find this asymmetry between the optimal serration and the worst serration is a common trend.

In Figure 6 we also plot an approximation to the ratio $P_f(1)/P_0(1)$ where we have calculated the integration with respect to z_0 analytically using the expression in Eq. (29). Here, we only plot up to $|\lambda| < 45°$, since this corresponds to $|w| = 2$ and $|f'(z)| < 1$. As well as needing shallow serrations for the Green's function, we also need the approximation in Eq. (29) to be valid. We can see that the analytic approximation agrees well with the numerical result in the region we have plotted it, although it does a lot worse outside it.

C. Effect of the parameters

Our next task is to look at the various parameters of the model and consider their effect on the reduction (or increase) in the scattered pressure. We have a lot of parameters to consider, with nine parameters for the eddy (amplitudes, Gaussian strengths and source), two for the serration (frequency, amplitude) and various parameters of the base flow (frequency ω, base flow velocity U, wavenumber k_0). We mainly focus on the eddy parameters since we are modelling the turbulence.

For the most part we will be fixing the amplitude and varying the frequency of the serration and comparing how the scattered pressure behaves for different eddy parameters. However, firstly we fix the eddy parameters and consider the effect of different amplitudes on the optimum serration. In Figure 7 we can see the effect of the different amplitudes on the power of the scattered pressure as we increase the frequency of the serrations. We have only plotted the range of frequencies such that $|f'(z)| < 1$. The trend to note from the graph is that as we reduce the amplitude of the serration then we reduce the effectiveness of the serrations (entirely as we expect), and furthermore the frequency of the optimum serration increases monotonically to a limit of around 5/6. This value will depend on the choice of the parameters of the eddy.

Next, we consider varying the parameters of the eddy. Since we have nine parameters of the eddy, we will vary each one in turn and consider the effectiveness of the serrations. We have different measures of effectiveness, for example do we fix a serration and measure how the power at this serration compares to the power of scattered pressure for a straight leading edge? Or do we look at the maximum reduction by calculating the infimum as below

$$\inf_{0<A<2} \frac{P_{A\sin(0.5z)}(\omega)}{P_0(\omega)}, \tag{33}$$

as we vary the eddy parameters? Or fixing the amplitude and taking an infimum over frequencies? We will choose the first measure because we would expect that in reality the serration would be fixed. Thus, to

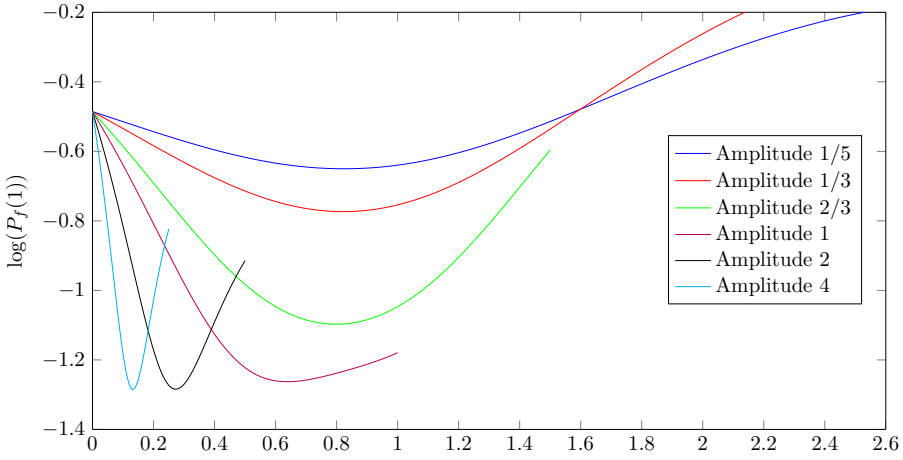

Figure 7: Plot of $P_f(1)$ for $f(z) = A\sin(wz)$ with different values of A. We have set $\omega = 1$, $c = 1$, $U_0 = 0.5$, $k_0 = 1$, $\boldsymbol{A} = (-1, 2, -2)$, $\boldsymbol{B} = (3, 1, 2)$ and $\boldsymbol{x}_e = (-3, 0, 1)$.

measure the effect of the serrations we consider the function

$$\mathbb{P}(\xi) = \frac{P_{\sin(0.5z),\xi}(\omega)}{P_{0,\xi}(\omega)}, \tag{34}$$

where ξ is one of the 9 parameters of the eddy, so $\xi \in \{x_e, y_e, z_e, A_1, A_2, A_3, B_1, B_2, B_3\}$. We have set $\omega = 1$, although we could choose to integrate over some region of ω space, avoiding 0 due to the singularity. We will fix the base parameters as

$$\boldsymbol{x}_e = (0, 0, 0), \quad \boldsymbol{A} = (1, 1, 1), \quad \boldsymbol{B} = (1, 1, 1), \tag{35}$$

and consider varying the eddy parameters in the ranges $-10 < A_i < 10$, $-10 < x_i < 10$ and $0 < B_i < 20$. This will be plotted in red in the following graphs. We also consider other interesting cases in different colours, where we will label which extra parameters we have changed. We could also have considered graphs in higher dimensions to show the effects of varying two or three parameters simultaneously.

In Figure 8 we have plotted a graph for each of the nine parameters of $\mathbb{P}(\xi)$ as the parameter varies, we require that $\mathbb{P}(\xi) < 1$ if the serration reduces the noise compared with a straight leading edge. The serration function is given by $f(z) = 0.5\sin(z)$.

The first graph, Figure 8a, shows that x_e has no effect on the power of the serration, which was clear from the form of $\mathcal{P}_s^f$ since the only dependence on x_e was the constant $\exp(-i\omega x_e/U)$. Physically speaking, this comes from the fact that the eddy has instantaneous amplitude and strength wherever it was created. Figure 8b shows the effect of y_e varying and is also entirely as we expect physically. As y_e moves away from 0 then the eddy is going above or below the aerofoil so the serrations have little or no effect, and we get the maximum noise reduction at $y_e = 0$. The extra spikes in the graph at $B_1 = 3$ and $A_2 = \pm 4$ where $\mathbb{P}(y_e) > 1$ are simply caused by $\sin(0.5z)$ no longer being the optimum serration, and we should choose a serration with smaller frequency.

Figure 8c shows the effect of varying z_e. This parameter plays a role since it changes at which point the eddy hits the serration, and as we saw in Section III.B this determines whether the serration reduces the noise or increases it. In the figure we see peaks and troughs, and these are exactly 4π apart, the wavelength of the serration. We also note that the amplitude of the graph changes, this stems from the fact that changing z_e actually shifts where the noise is centred. Since we are integrating between $[-6\pi, 6\pi]$, which is centred at zero the power of the scattered pressure changes. If we were instead integrating over $[z_e - 6\pi, z_e + 6\pi]$ then we would expect the amplitude to be constant. We also have a third effect happening when $A_3 = 1$ and $y_e = 1$, where there is some damping on the maximum amplitude, and in the latter case this actually turns what should be peaks into troughs. This effect definitely needs to be investigated further but can probably be discarded since when $y_e = 1$ the effect of the eddy is minimal, as seen in Figure 8b.

In Figure 8d we see how $\mathbb{P}(A_1)$ varies. We see that for positive A_1 there is an optimum amplitude (around $A_1 = 0.3$) where $\mathbb{P}(A_1)$ is minimised. As A_1 increases from 0.3 to infinity then $\mathbb{P}(A_1) \uparrow 1$, and hence we are

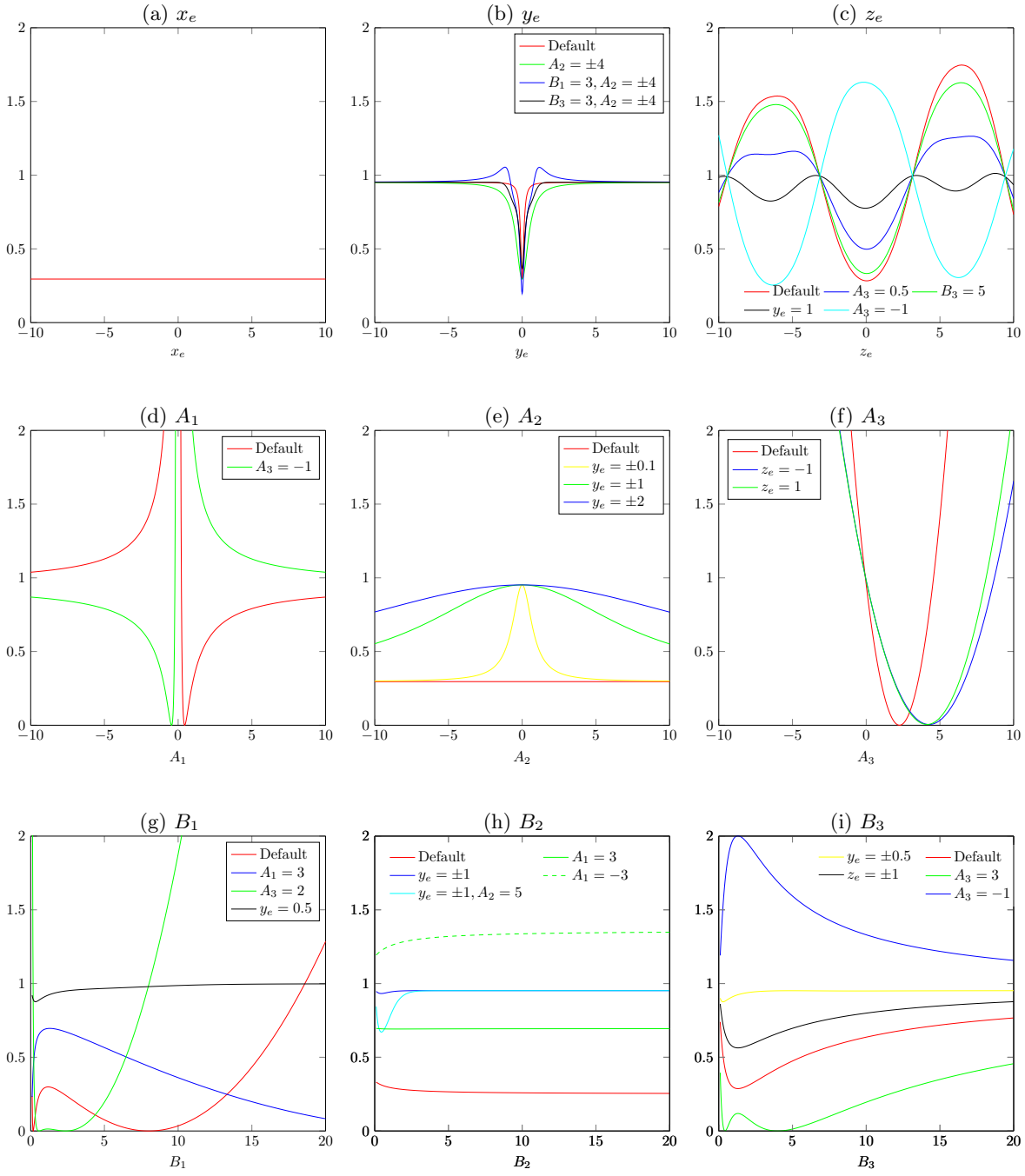

Figure 8: Effect of the parameters on $\mathbb{P}(\xi)$, we need $\mathbb{P}(\xi) < 1$ to reduce the noise.

still reducing the noise for the serration $f(z)$ compared with a straight leading edge. When we consider the limit $A_1 \downarrow 0$ then $\mathbb{P}(A_1) \to \infty$, this is because the eddy is becoming parallel to a straight leading edge. Thus, the frequency of the optimum serration tends to 0, as a result $f(z)$ is not at all optimum and this causes $\mathbb{P}$ to increase above 1 and no longer reduce the noise. When A_1 is negative we can see that we always have $\mathbb{P}(A_1) > 1$, and the shape of the graph can be explained by the same reasoning as above. Setting $A_3 = -1$ changes the graph in exactly the way we would expect, since now we need A_1 to also be negative if we were to reduce the noise and A_1 positive to increase the noise.

Figure 8e shows the effect of changing the amplitude of the eddy in the y direction. Unsurprisingly, when the eddy is centred is $y_e = 0$ this has no effect, but as the eddy moves above or below the aerofoil then it changes the effectiveness of the serration. As the amplitude A_2 increases in modulus then the serration $f(z)$ become more effective at reducing the noise (so $\mathbb{P}$ reduces), although the effectiveness levels off to the value in the case $y_e = 0$. Larger values of y_e reduce the gradient of $\mathbb{P}$ as can be seen clearly in the figure. In Figure 8f we see what role A_3 plays on the effectiveness of the serration $f(z)$. There is an optimum amplitude A_3 at which the serrated leading edge $f(z)$ reduces the scattered pressure to close to zero. This optimum amplitude is dependent on the parameters as can be seen, and for the default parameters is at around $A_3 = 2.25$. As we increase the amplitude past this point the noise from the serrated edge increases, until eventually it becomes louder than the straight leading edge (at $A_3 = 4.5$). This is simply because we should be choosing a serration with a smaller frequency to reduce the noise. As A_3 goes below zero then we actually increase the noise compared with a straight edge, since now the eddy hits the serration at the wrong angle as we saw in Figure 8d. Looking at different values of z_e simply changes the optimum amplitude, at which $\mathbb{P}$ is minimised.

Finally, we consider Figures 8g, 8h and 8i. These show the effect of changing the strengths of the Gaussian in the three different directions. Note that we have problems close to 0 for B_1 and B_3, this stems from the fact that we divide by both γ_{11} and γ_{33} to calculate the scattered pressure. The three figures show that for a fixed serration and fixed other parameters, there is an optimal Gaussian strength in each direction. In Figure 8g we can see that as we increase the Gaussian strength B_1 our serration $f(z)$ no longer necessary reduces the noise, this is just because the optimal serration changes. In Figures 8h and 8i the serrated leading edge always reduces noise compared with a straight edge, except for the cases where $A_1 = -3$ in Figure 8h and $A_3 = -1$ in Figure 8i, which we discussed in the previous section. We also notice that as we increase the Gaussian strengths to infinity, the effectiveness of the serrations $\mathbb{P}$ tends to a limit. In Figure 8h this limit depends on the parameters, while in Figure 8i the limit is 1.

D. Two eddies

We next seek to understand the effect of turbulence interacting with the leading edge when the turbulence consists of two eddies. Because of the form of the Navier–Stokes equation in Eq. (16) we know that the two eddies will interact with each other in a nonlinear way. We assume both of the eddies have Gaussian profiles, as opposed to Haeri et al[1] where they also considered Mexican hat profiles. We find that when the eddies have the same source but different amplitudes and Gaussian strengths we can perform the calculation relatively easily and the number of terms increases from four to sixteen as we would expect. When the eddies have different sources it is more complicated and we get significantly more terms as we will see below.

1. Same sources

To fix ideas, we assume that the perturbation velocity is given by

$$\boldsymbol{u}(\boldsymbol{x},t) = \nabla \times \left[\boldsymbol{\Phi}(\boldsymbol{x},t) + \boldsymbol{\Psi}(\boldsymbol{x},t)\right], \tag{36}$$

where we have

$$\boldsymbol{\Phi}(\boldsymbol{x},t) = A_1 e^{-B_1 R}\boldsymbol{e}_x + A_2 e^{-B_2 R}\boldsymbol{e}_y + A_3 e^{-B_3 R}\boldsymbol{e}_z, \tag{37}$$

and

$$\boldsymbol{\Psi}(\boldsymbol{x},t) = C_1 e^{-D_1 R}\boldsymbol{e}_x + C_2 e^{-D_2 R}\boldsymbol{e}_y + C_3 e^{-D_3 R}\boldsymbol{e}_z, \tag{38}$$

where R is defined in Eq. (13) and is the same for both eddies. After a calculation similar to Section III.A, we conclude that

$$\mathcal{P}_s(\boldsymbol{x},\omega) = A\sqrt{r^*}\sin(\theta^*/2)\int_{-\infty}^{\infty}\frac{e^{ik_0|\boldsymbol{x}-\boldsymbol{z}_s|}}{|\boldsymbol{x}-\boldsymbol{z}_s|^{3/2}}Q^{\mathrm{ii}}(z_0,\omega)\mathrm{d}z_0, \tag{39}$$

where A is the constant given in Eq. (23) and Q^{ii} is given by the lengthy formula

$$\begin{aligned}
Q^{\mathrm{ii}}(z_0,\omega) &= (z_0-z_e)Q^*_{\beta^{AB}_{23},\gamma^B_{23}}(z_0,\omega) + y_e Q^*_{\beta^{AB}_{11},\gamma^B_{11}}(z_0,\omega) + y_e Q^*_{\beta^{AB}_{33},\gamma^B_{33}}(z_0,\omega) - \frac{i\omega}{2\gamma^B_{12}U} Q^*_{\beta^{AB}_{12},\gamma^B_{12}}(z_0,\omega) \\
&+ (z_0-z_e)Q^*_{\beta^{CD}_{23},\gamma^D_{23}}(0z_0,\omega) + y_e Q^*_{\beta^{CD}_{11},\gamma^D_{11}}(z_0,\omega) + y_e Q^*_{\beta^{CD}_{33},\gamma^D_{33}}(z_0,\omega) - \frac{i\omega}{2\gamma^D_{12}U} Q^*_{\beta^{CD}_{12},\gamma^D_{12}}(z_0,\omega) \\
&+ (z_0-z_e)Q^*_{\beta^{AD}_{32},\gamma^{BD}_{32}}(z_0,\omega) + y_e Q^*_{\beta^{AD}_{11},\gamma^{BD}_{11}}(z_0,\omega) + y_e Q^*_{\beta^{AD}_{33},\gamma^{BD}_{33}}(z_0,\omega) - \frac{i\omega}{2\gamma^{BD}_{12}U} Q^*_{\beta^{AD}_{12},\gamma^{BD}_{12}}(z_0,\omega) \\
&+ (z_0-z_e)Q^*_{\beta^{AD}_{23},\gamma^{BD}_{23}}(z_0,\omega) + y_e Q^*_{\beta^{AD}_{11},\gamma^{BD}_{11}}(z_0,\omega) + y_e Q^*_{\beta^{AD}_{33},\gamma^{BD}_{33}}(z_0,\omega) - \frac{i\omega}{2\gamma^{BD}_{21}U} Q^*_{\beta^{AD}_{21},\gamma^{BD}_{21}}(z_0,\omega).
\end{aligned} \tag{40}$$

In this equation $Q^*_{\beta,\gamma}$ is given by Eq. (26), and the constants β and γ are given by

$$\beta^{AB}_{ij} = A_iB_iA_jB_j, \quad \beta^{CD}_{ij} = C_iD_iC_jD_j, \qquad \beta^{AD}_{ij} = A_iB_iC_jD_j, \tag{41}$$

and

$$\gamma^B_{ij} = B_i + B_j, \quad \gamma^D_{ij} = D_i + D_j, \quad \gamma^{BD}_{ij} = B_i + D_j. \tag{42}$$

Note that while $\beta^{AB}_{ij} = \beta^{AB}_{ji}$, $\beta^{AD}_{ij} \neq \beta^{AD}_{ji}$, and thus the last two lines of Q^{ii} are not the same. We will next consider the more interesting (and realistic) case when the sources of the two eddies are allowed to differ.

2. Different sources

When we have different sources we have two different form of R, let us define them as

$$R^\Psi = (x - x^\Psi_e - Ut)^2 + (y-y^\Psi_e)^2 + (z-z^\Psi_e)^2 \text{ and } R^\Phi = (x - x^\Phi_e - Ut)^2 + (y-y^\Phi_e)^2 + (z-z^\Phi_e)^2, \tag{43}$$

where the eddy associated to $\mathbf{\Phi}$ has source $(x^\Phi_e, y^\Phi_e, z^\Phi_e)$ and similar for $\mathbf{\Psi}$. We define the distance between the sources to be $\boldsymbol{\varepsilon} = (\varepsilon_x, \varepsilon_y, \varepsilon_z) = (x^\Phi_e - x^\Psi_e, y^\Phi_e - y^\Psi_e, z^\Phi_e - z^\Psi_e)$. We can calculate that the scattered pressure will be of the form

$$\mathcal{P}_s(\boldsymbol{x},\omega) = A\sqrt{r^*}\sin(\theta^*/2)\int_{-\infty}^{\infty} \frac{e^{ik_0|\boldsymbol{x}-\boldsymbol{z}_s|}}{|\boldsymbol{x}-\boldsymbol{z}_s|^{3/2}} \left(Q^{\mathrm{II}}(z_0,\omega) + 2Q^D(z_0,\omega)\right) \mathrm{d}z_0, \tag{44}$$

where the constant A is independent of the serration and given by (23), Q^{II} is given by a similar form to Eq. (40) and Q^D remains to be found. We define the terms

$$Q^\Phi_{ij}(z_0,\omega) = \frac{U^{1/2}}{2\omega}\frac{\beta^{AB}_{ij}\pi e^{3\pi i/4}}{\sqrt{\gamma^B_{ij}}} e^{-\gamma^B_{ij}y_e^{\Phi\,2}} e^{-\omega^2/(4\gamma^B_{ij}U^2)} e^{-i\omega x^\Phi_e/U} e^{-\gamma^B_{ij}(z_0-z^\Phi_e)^2} e^{i\omega f(z_0)/U}, \tag{45}$$

$$Q^\Psi_{ij}(z_0,\omega) = \frac{U^{1/2}}{2\omega}\frac{\beta^{CD}_{ij}\pi e^{3\pi i/4}}{\sqrt{\gamma^D_{ij}}} e^{-\gamma^D_{ij}y_e^{\Psi\,2}} e^{-\omega^2/(4\gamma^D_{ij}U^2)} e^{-i\omega x^\Psi_e/U} e^{-\gamma^D_{ij}(z_0-z^\Psi_e)^2} e^{i\omega f(z_0)/U}, \tag{46}$$

and

$$\begin{aligned}
Q^{\Phi,\Psi}_{ij}(z_0,\omega) = \frac{U^{1/2}}{2\omega}\frac{\beta^{AD}_{ij}\pi e^{3\pi i/4}}{\sqrt{\gamma^{BD}_{ij}}} & e^{-B_iy_e^{\Phi\,2} - D_jy_e^{\Psi\,2}} e^{-\omega^2/(4\gamma^{BD}_{ij}U^2)} e^{-B_i(z_0-z^\Phi_e)^2 - D_j(z_0-z^\Psi_e)^2} e^{i\omega f(z_0)/U} \\
&\times \exp\left(\frac{-i\omega}{U\gamma^{BD}_{ij}}[B_ix^\Phi_e + D_jx^\Psi_e]\right) \exp\left(\frac{B_iD_j}{\gamma^{BD}_{ij}}\left[2x^\Psi_e x^\Phi_e - x_e^{\Psi\,2} - x_e^{\Phi\,2}\right]\right).
\end{aligned} \tag{47}$$

and then

$$
\begin{aligned}
Q^{\mathrm{II}}(z_0,\omega) &= (z_0 - z_e^{\Phi})Q_{23}^{\Phi}(z_0,\omega) + y_e^{\Phi}Q_{11}^{\Phi}(z_0,\omega) + y_e^{\Phi}Q_{33}^{\Phi}(z_0,\omega) - \frac{i\omega}{2\gamma_{12}^{B}U}Q_{12}^{\Phi}(z_0,\omega) \\
&+ (z_0 - z_e^{\Psi})Q_{23}^{\Psi}(z_0,\omega) + y_e^{\Psi}Q_{11}^{\Psi}(z_0,\omega) + y_e^{\Psi}Q_{33}^{\Psi}(z_0,\omega) - \frac{i\omega}{2\gamma_{12}^{D}U}Q_{12}^{\Psi}(z_0,\omega) \\
&+ (z_0 - z_e^{\Psi})Q_{32}^{\Phi,\Psi}(z_0,\omega) + (y_e^{\Phi} + y_e^{\Psi})Q_{11}^{\Phi,\Psi}(z_0,\omega) + \left[-\frac{i\omega}{2\gamma_{12}^{BD}U} + \frac{\varepsilon_x B_1}{\gamma_{12}^{BD}}\right] Q_{12}^{\Phi,\Psi}(z_0,\omega) \\
&+ (z_0 - z_e^{\Phi})Q_{23}^{\Phi,\Psi}(z_0,\omega) + (y_e^{\Phi} + y_e^{\Psi})Q_{33}^{\Phi,\Psi}(z_0,\omega) + \left[-\frac{i\omega}{2\gamma_{21}^{BD}U} - \frac{\varepsilon_x D_1}{\gamma_{21}^{BD}}\right] Q_{21}^{\Phi,\Psi}(z_0,\omega). \qquad (48)
\end{aligned}
$$

The term Q^D is given in Eq. (65) in the Appendix A, as are the necessary integrals needed to calculate both Q^{II} and Q^D. In the limit of $\boldsymbol{\varepsilon} \to 0$ we can see that $Q^D \to 0$ and thus we recover the approximation for two eddies with the same source. Note that the first two terms of Q are the linear terms, which we get by adding the single eddy results for the eddies $\boldsymbol{\Phi}$ and $\boldsymbol{\Psi}$. The third and fourth terms are the quadratic terms, while the Q^D term can be viewed as some correction to the third and fourth terms due to them having different sources.

E. Multiple eddies

It is clear that our approach for considering two eddies can easily be extended to N eddies, since we just need to deal with the cross terms between any two eddies. For N eddies the Q terms will consist of N^2 terms, while the numbers of terms in the Q^D term will be $N(N-1)/2$ times the number of terms in Eq. (65). We will compare the full approximation (the integral of $Q + 2R$), the quadratic approximation (the integral of Q) and the linear approximation (the integral of the first N terms of Q). The linear approximation is just the sum of the one eddy results for each of the N eddies. It is clear that to generate turbulence we need to generate the amplitudes, Gaussian distributions and source positions of each eddy stochastically.

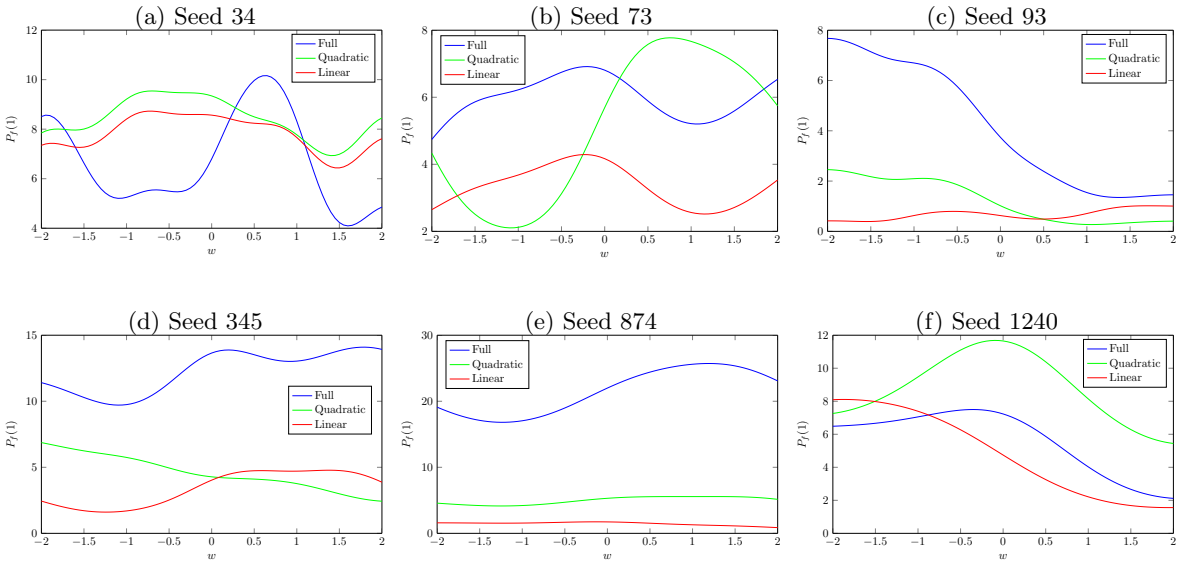

Figure 9: Plot of $P_f(1)$ against serration $f(z) = 0.5\sin(wz)$ for six randomly generated turbulence fields. Each of them is created with a different seed.

The model we use is a normal distribution (with zero mean and unit standard deviation) for the amplitudes and source positions, while the Gaussian strengths of the eddies are chosen uniformly in $[1, 5]$. In Haeri et al[1] they only state that the Gaussian strengths are between R_{min} and R_{max} (which in turn depend on the chord length of the aerofoil), with no information given about the parameters of the eddy except it is chosen such that is satisfies the von Kármán energy. This is given in Wilson.[9] In Figure 9 we have randomly

generated ten eddies, and each of the figures corresponds to a different random seed. We stick to $N = 10$ for computational time, but it is easy to extend to higher values of N.

The underlying message from the figure is that even with ten eddies we can reduce the noise by introducing a leading-edge serration, however it is not clear what the serration should be unless we know the eddy parameters. The optimal serration varies depending on the eddy parameters, and it is clear there is no one optimal serration which works for all the eddy parameters. We also see that for the six cases in Figure 9 the linear and quadratic approximations generally approximates the minima of P_f quite well in comparison to the full approximation.

In Figures 9b and 9d we can see that the linear approximation is very good, and the quadratic approximation is quite poor. In Figures 9c, 9e and 9f we can see the quadratic approximation does very well while this time the linear approximation does poorly. Having said that, in Figure 9f all three approximations agree that to reduce the noise the most we should choose a serration with frequency $w = 2$. In Figure 9a we can see that for once the linear and quadratic approximations are quite close, and although they do not agree entirely with the general shape of the full approximation, all three approximations suggest the optimal serration should have a frequency of around $w = 1.5$.

Thus, we have shown we can randomly generate turbulence corresponding to N eddies analytically and still find an optimal leading-edge serration that reduces the noise compared with a straight leading edge. Furthermore this optimal serration depends on the parameters of the N eddies.

IV. Angle of attack

Our final consideration is to consider the serrated aerofoil at a small angle of attack α to the flow. We restrict to small angles of attack, because then we can continue to use $(U, 0, 0)$ as the base flow, and for larger angle of attack this would clearly change to allow base flow in the y direction. We can calculate the scattered pressure is given by

$$\mathcal{P}_s^{f,\alpha}(\boldsymbol{x},\omega) = -\int_{-\infty}^{\infty}\int_{0}^{\infty}\left\{\sin\alpha\frac{\partial\mathcal{P}_i}{\partial x}(\boldsymbol{x}_1;\omega) + \cos\alpha\frac{\partial\mathcal{P}_i}{\partial y}(\boldsymbol{x}_1;\omega)\right\}[G^{f,\alpha}(\boldsymbol{x}, x_1 + f(z_0), z_0;\omega)]\mathrm{d}x_1\mathrm{d}z_0, \quad (49)$$

where

$$\boldsymbol{x}_1 = (x_1 + \cos\alpha f(z_0), -\tan\alpha x_1 - \sin\alpha f(z_0), z_0), \quad (50)$$

and $[G^{f,\alpha}]$ is the Green's function for an aerofoil with leading-edge serration $f(z)$ at angle of attack α.

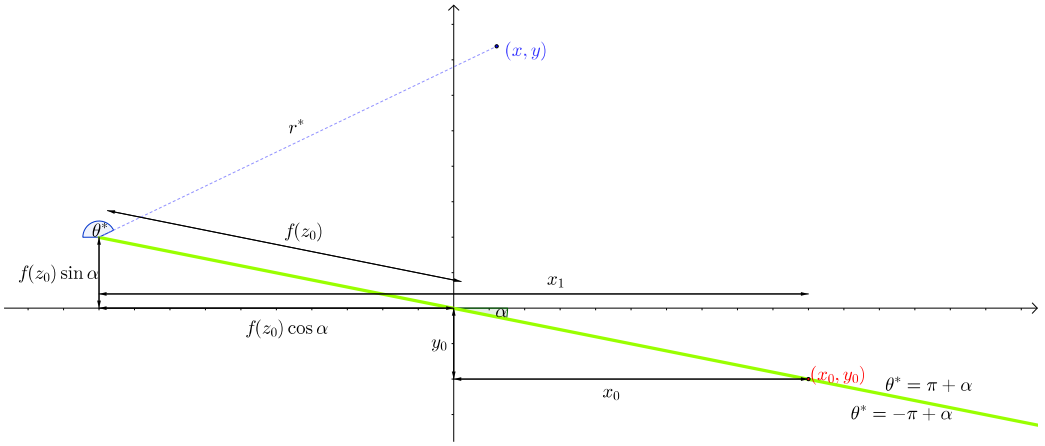

Figure 10: Description of the geometry of the problem (where $f(z_0)$ is negative in the picture.)

A. Coordinate system

We introduce a modified serrated coordinate system $(r^\star, \theta^\star, z^\star)$ where $r^\star$ is distance the to the leading edge of the aerofoil, and $\theta^\star$ is the angle from the tip of the aerofoil, with $\theta^\star = 0$ corresponding to

the line ($x < f(z_0)\cos\alpha, y = -f(z)\sin\alpha$), which is shown in Figure 10. Note that in terms of Cartesian coordinates the modified serrated coordinates are given by

$$(x, y, z) = (f(z^\star)\cos\alpha - r^\star\cos\theta^\star, -f(z^\star)\sin\alpha - r^\star\sin\theta^\star, z^\star). \tag{51}$$

In the new coordinate system, for a general point on the aerofoil $(x_0, -\tan\alpha x_0)$ we have

$$r_0^\star = x_0\sec\alpha - f(z_0) = x_1\sec\alpha. \tag{52}$$

For a general point (x, y) we have

$$r^\star = \sqrt{(x - f(z_0)\cos\alpha)^2 + (y - f(z_0)\sin\alpha)^2}. \tag{53}$$

B. Green's function

FOR a serrated leading edge we can calculate that the jump of the Green's function is approximately given by

$$[G^{f,\alpha}(\boldsymbol{x}, x_1 + f(z_0), z_0; \omega)] = -\frac{2\sqrt{k_0}}{\pi\sqrt{2\pi i}}\sqrt{r^\star}\sin\left(\frac{\theta^\star}{2} - \frac{\alpha}{2}\right)\frac{e^{ik_0|\boldsymbol{x}-\boldsymbol{z}_s|}}{|\boldsymbol{x}-\boldsymbol{z}_s|^{3/2}}\left(x_1\sec\alpha\right)^{1/2}, \tag{54}$$

which is calculated in the same way as in Section II.D. Recall that $|\boldsymbol{x} - \boldsymbol{z}_s| = r^{\star 2} + (z - z_0)^2$. The terms that have changed in comparison with Eq. (9) to are a factor of $\sec^{1/2}\alpha$ and the sin term now differs by α. However, the big difference in the calculation of the scattered pressure is actually the pressure terms; there are now two of them and they will have more complicated dependence on x_0.

C. Calculating the pressure

USING the same method as in Section III.A we can calculate that

$$\frac{\partial\mathcal{P}_i}{\partial y}(x, y, z, \omega) = \frac{-2\rho_0}{U\sqrt{\pi}}\left[\beta_{23}(z - z_e)\mathbb{E}_{\gamma_{23}} + \beta_{11}(y_e - y)\mathbb{E}_{\gamma_{11}} + \beta_{33}(y_e - y)\mathbb{E}_{\gamma_{33}} - \frac{i\omega}{2\gamma_{12}U}\beta_{12}\mathbb{E}_{\gamma_{12}}\right], \tag{55}$$

and

$$\frac{\partial\mathcal{P}_i}{\partial x}(x, y, z, \omega) = \frac{-2\rho_0}{U\sqrt{\pi}}\left[\beta_{12}(y - y_e)\mathbb{E}_{\gamma_{12}} + \beta_{13}(z - z_e)\mathbb{E}_{\gamma_{13}} + \frac{i\omega}{2\gamma_{22}U}\beta_{22}\mathbb{E}_{\gamma_{22}} + \frac{i\omega}{2\gamma_{33}U}\beta_{33}\mathbb{E}_{\gamma_{33}}\right], \tag{56}$$

where we have dropped the dependence of $\mathbb{E}_\gamma$ on $\boldsymbol{x}$ and ω to save space; $\mathbb{E}_\gamma$ consists of various exponential terms and is given by

$$\mathbb{E}_\gamma(\boldsymbol{x}, \omega) = \frac{1}{\sqrt{\gamma}}e^{-\gamma(z-z_e)^2}e^{-\gamma(y-y_e)^2}e^{i\omega(x-x_e)/U}e^{-\omega^2/(4\gamma U^2)}. \tag{57}$$

Note that the definition of $\mathbb{E}$ in Eq. (57) agrees with the definition in Eq. (21) when $y = 0$, so at zero angle of attack. The scattered pressure is then given by

$$\mathcal{P}_s^{f,\alpha}(\boldsymbol{x}, \omega) = A\sqrt{r^\star}\sin\left(\frac{\theta^\star}{2} - \frac{\alpha}{2}\right)\int_{-\infty}^{\infty}\frac{e^{ik_0|\boldsymbol{x}-\boldsymbol{z}_s|}}{|\boldsymbol{x}-\boldsymbol{z}_s|^{3/2}}\left[\sin\alpha Q^x(z_0, \omega) + \cos\alpha Q^y(z_0, \omega)\right]\mathrm{d}z_0, \tag{58}$$

where A has been defined before in Eq. (23) and

$$Q^i(z_0, \omega) = -\frac{\pi\omega^{1/2}}{2\rho_0}\int_0^\infty x_1^{1/2}\left(\nabla\mathcal{P}_i\right)_i\left(x_1 + \cos\alpha f(z_0), -\tan\alpha x_1 - \sin\alpha f(z_0), z_0, \omega\right)\mathrm{d}x_1. \tag{59}$$

Defining

$$Q^\star_{\beta,\gamma}(z_0, \omega) = \frac{\beta\sqrt{\pi}}{\sqrt{\gamma}U}e^{-\gamma y_e^2}e^{-\omega^2/(4\gamma U^2)}e^{-i\omega x_e/U}e^{-\gamma(z_0-z_e)^2}e^{i\omega\cos\alpha f(z_0)/U}, \tag{60}$$

and

$$I^n_\gamma(z_0, \omega) = \int_0^\infty x_1^n e^{i\omega x_1/U}\exp[-\gamma\tan^2\alpha\left(x_1 + \cos\alpha f(z_0) + \cot\alpha y_e\right)^2]\mathrm{d}x_1, \tag{61}$$

then gives

$$Q^x(z_0,\omega) = (z_0 - z_e)Q^\star_{\beta_{13},\gamma_{13}} I^{1/2}_{\gamma_{13}} + \frac{i\omega}{2\gamma_{22}U} Q^\star_{\beta_{22},\gamma_{22}} I^{1/2}_{\gamma_{22}} + \frac{i\omega}{2\gamma_{33}U} Q^\star_{\beta_{33},\gamma_{33}} I^{1/2}_{\gamma_{33}} - J_{\gamma_{12}} Q^\star_{\beta_{12},\gamma_{12}}, \tag{62}$$

and

$$Q^y(z_0,\omega) = (z_0 - z_e)Q^\star_{\beta_{23},\gamma_{23}} I^{1/2}_{\gamma_{23}} - \frac{i\omega}{2\gamma_{12}U} Q^\star_{\beta_{12},\gamma_{12}} I^{1/2}_{\gamma_{12}} + J_{\gamma_{11}} Q^\star_{\beta_{11},\gamma_{11}} + J_{\gamma_{33}} Q^\star_{\beta_{33},\gamma_{33}}, \tag{63}$$

where

$$J_\gamma(z_0,\omega) = (y_e + \sin\alpha f(z_0))\, I^{1/2}_\gamma(z_0,\omega) + \tan\alpha I^{3/2}_\gamma(z_0,\omega). \tag{64}$$

We have dropped the dependence of I^n_γ, J_γ and $Q^\star_{\beta,\gamma}$ on (z_0,ω) to simplify the notation. The integrals $I^{1/2}_\gamma$ and $I^{3/2}_\gamma$ can actually be calculated analytically, and this is detailed in Appendix B. We no longer need to use the theory of generalised integrals (unless $\alpha = 0$) and we get results in term of modified Bessel functions. We can check that when $\alpha = 0$ we recover the previous result in Section III.A.

D. Results

In Figure 11 we can see the comparison of the scattered pressure between a straight leading edge and a serrated leading edge. We again see a noticeable reduction in the noise, even at angle of attack $\alpha = \pi/30$ (6°), and our serration still remains shallow (with $|f'(z)| < 3/8$).

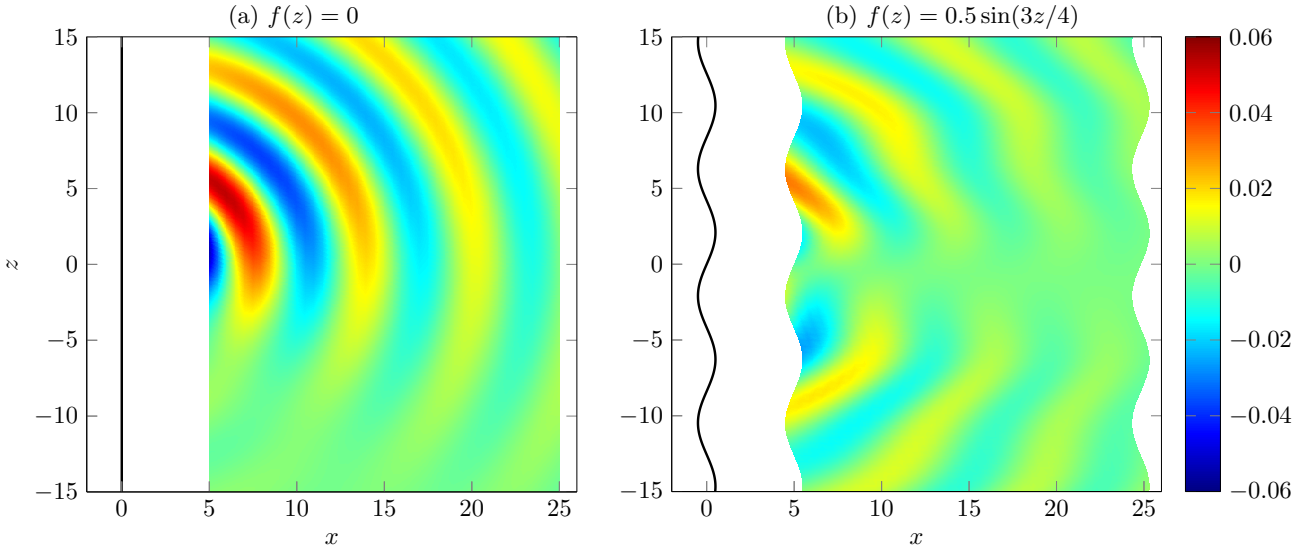

Figure 11: Plot of real part of $\mathcal{P}^{f,\alpha}_s(\boldsymbol{x},\omega)/A$ for non serrated and serrated edge at angle of attack $\alpha = \pi/30$ (6°) and $\theta^\star = \pi + \alpha$. We have set $\omega = 1$, $c = 1$, $U_0 = 0.5$ and $k_0 = 1$. Additionally the eddy parameters are $\boldsymbol{A} = (1,2,1)$, $\boldsymbol{B} = (1,1,2)$ and $\boldsymbol{x}_e = (-2,0,0)$.

Measuring the power of the scattered pressure as before, we can see how the pressure varies across different angle of attacks and different leading-edge serrations in Figure 12. We have fixed the eddy parameters and are only changing the angle of attack from 0 to $\pi/20$ (9°). In the figure we have chosen y_e non-zero, since otherwise we get problems for serrations with frequencies close to zero. This only occurs at higher angle of attacks and is mostly likely just an implementation issue. We see two features from the figure.

The first is that the maximum noise reduction becomes smaller as the angle of attack increases, which is entirely what we expect. At higher angle of attacks, less of the serrations are in line with the base flow and thus effectively the serrations have lower amplitudes. It is worth noticing that by the time we have got to angle of attack $\pi/20$, the effect of serrations is negligible in reducing the noise. We can see in Table 1 exactly how much we can reduce the noise to, as a percentage of the noise of a straight edge. Of course these values will depend on the parameters of the eddy.

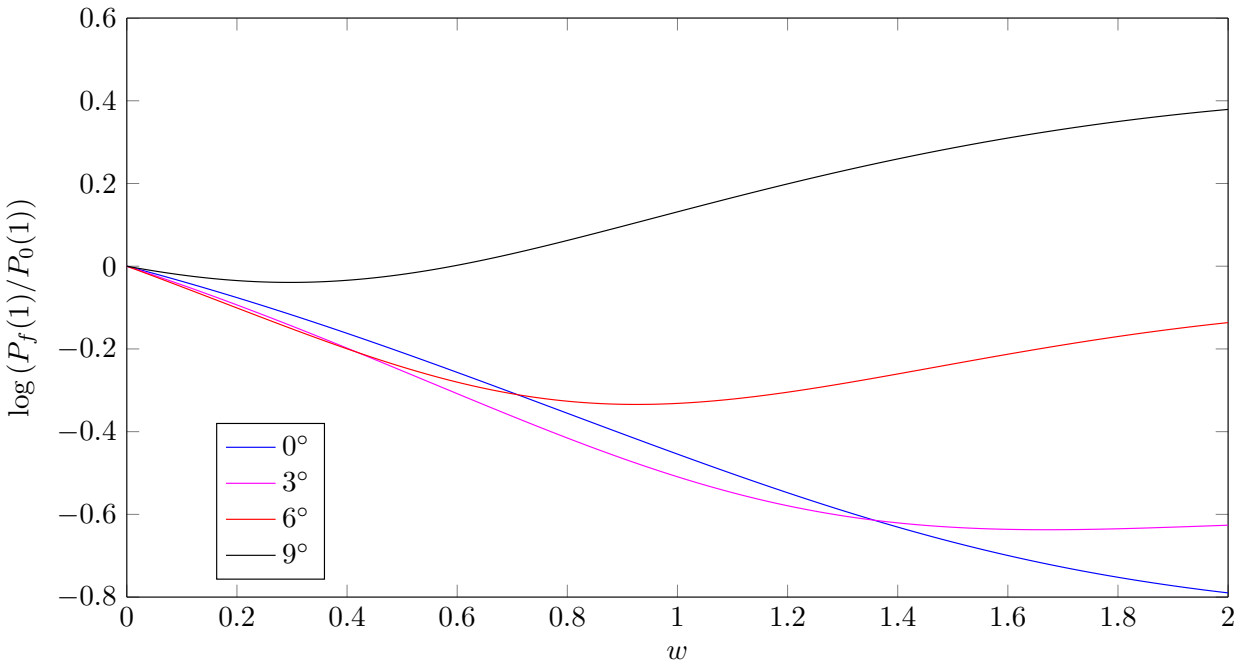

Figure 12: Graph of $P_f(1)$ for $f(z) = \sin(wx)$ with different angle of attack. We have set $\omega = 1$, $c = 1$, $U_0 = 0.5$ and $k_0 = 1$. Additionally the eddy parameters are $\boldsymbol{A} = (1, 2, 1)$, $\boldsymbol{B} = (1, 1, 2)$ and $\boldsymbol{x}_e = (-2, 0.1, 0)$.

Angle of attack (°)	Maximum reduction in noise	Value of w achieved at
0	45.4%	2
3	52.9%	1.67
6	71.6%	0.93
9	96.2%	0.30

Table 1: Table showing how the maximum reduction in noise varies with angle of attack. The maximum reduction is a percentage of the noise at the leading edge. The eddy paramaters are the same as that in Figure 12.

The second feature is that the value of w for the optimum serration $f(z) = \sin(wz)$ (to maximise the noise reduction) reduces as the angle of attack increases up to $\pi/20$. This is perhaps not unexpected, but further adds weight to the conclusion that we would need to allow the serration to vary for it to be effective at reducing the noise compared with a straight leading edge.

V. Conclusion and future work

We have investigated the effect of leading-edge serrations on the scattered pressure when our turbulence is driven by a number of eddies. We have shown that we are able to reduce the scattered pressure, even when we have multiple eddies which were randomly determined. We also showed that we can extend this to small angles of attack. However, predicting the optimum level of serrations is very difficult. In essence, allowing the eddies to be random causes the optimal serration to be somewhat stochastic. We can not hope that one serration will reduce the noise for all parameters of the eddies, this is clearly shown in Sections III.C and III.E. Instead, the best we can hope for is that the leading-edge serration reduces the noise "most" of the time. In an ideal world we would allow the leading-edge serration on the aerofoil to dynamically vary, but how feasible this would be in the future is unknown.

The main limitations of our model were that the leading-edge serration was shallow and that we were in

high Reynolds number, low Mach number flow. Also, our results are only valid in the far field. It was argued by Howe[3] that in the case of a general serration we get an upper bound on pressure, although this may no longer be true since we considered a different model of turbulence. We imposed the conditions on the flow so that our governing equation was simple enough to calculate the Green's function. If we considered lower Reynolds number or higher Mach numbers we need to take into account convection and scattering by the flow. The governing equation would then be significantly more complicated and the Green's function would be fundamentally altered, if it can be found analytically at all. The far-field approximation is needed to allow us to make any analytical progress with the Green's function, and furthermore is a sensible approximation because the observer will be in the far field of the aerofoil except at take off and landing.

In the future we want to model the aerofoil geometry more realistically. We aim to investigate features such as finite chord length, finite span and non zero thickness and shape of the aerofoil. It is likely that finding an analytic Green's function which takes into account all these features is beyond us, but we can certainly make some progress. Changing to a finite chord involves changing the boundary conditions for the Green's function, and one way of calculating the Green's function is to add a leading and a trailing edge Green's function together, with the method of images used to get the correct boundary conditions. This would also allow us to consider different serrations on the leading and trailing edge of the aerofoil, as seen in Figure 1a. Some work has already been done on a finite chord by Howe,[10] although a different form of turbulence was considered. A finite span could perhaps be treated in a similar manner. To investigate shape and thickness of the aerofoil, we could introduce coordinates which map the aerofoil back to being a thin plate, as considered by Ayton and Peake.[11]

Appendix

A. Analytical calculation of pressure for two eddies with different sources

The term Q^D is given by the following expression

$$
\begin{aligned}
Q^D(z_0,\omega) = {} & B_1(z_0 - z_e^{\Phi}) Q_{13}^{\Phi,\Psi}(z_0,\omega) \left[\varepsilon_y \frac{i\omega}{2\gamma_{13}^{BD} U} - \varepsilon_x \frac{B_1 y_e^{\Phi} + D_3 y_e^{\Psi}}{\gamma_{13}^{BD}} \right] \\
& - D_1(z_0 - z_e^{\Psi}) Q_{31}^{\Phi,\Psi}(z_0,\omega) \left[\varepsilon_y \frac{i\omega}{2\gamma_{31}^{BD} U} - \varepsilon_x \frac{B_3 y_e^{\Phi} + D_1 y_e^{\Psi}}{\gamma_{31}^{BD}} \right] \\
& + D_1(z_0 - z_e^{\Psi}) Q_{21}^{\Phi,\Psi}(z_0,\omega) \left[\varepsilon_z \frac{i\omega}{2\gamma_{21}^{BD} U} + \varepsilon_x z_0 - \varepsilon_x \frac{B_2 z_e^{\Phi} + D_1 z_e^{\Psi}}{\gamma_{21}^{BD}} \right] \\
& - B_1(z_0 - z_e^{\Phi}) Q_{12}^{\Phi,\Psi}(z_0,\omega) \left[\varepsilon_z \frac{i\omega}{2\gamma_{12}^{BD} U} + \varepsilon_x z_0 - \varepsilon_x \frac{B_1 z_e^{\Phi} + D_2 z_e^{\Psi}}{\gamma_{12}^{BD}} \right] \\
& + (B_3 - D_3) Q_{33}^{\Phi,\Psi}(z_0,\omega) \left[\frac{\varepsilon_y}{2\gamma_{33}^{BD}} + \frac{i\omega}{2\gamma_{33}^{BD} U} \left(\varepsilon_y \frac{i\omega}{2\gamma_{33}^{BD} U} - \varepsilon_x \frac{B_3 y_e^{\Phi} + D_3 y_e^{\Psi}}{\gamma_{33}^{BD}} \right) \right] \\
& + \varepsilon_x \frac{2B_3 D_3}{\gamma_{33}^{BD}} Q_{33}^{\Phi,\Psi}(z_0,\omega) \left(\varepsilon_y \frac{i\omega}{2\gamma_{33}^{BD} U} - \varepsilon_x \frac{B_3 y_e^{\Phi} + D_3 y_e^{\Psi}}{\gamma_{33}^{BD}} \right) \\
& + D_3 Q_{23}^{\Phi,\Psi}(z_0,\omega) \left[\frac{\varepsilon_z}{2\gamma_{23}^{BD}} + \left(\frac{i\omega}{2\gamma_{23}^{BD} U} - \varepsilon_x \frac{B_2}{\gamma_{23}^{BD}} \right) \left(\varepsilon_z \frac{i\omega}{2\gamma_{23}^{BD} U} + \varepsilon_x z_0 - \varepsilon_x \frac{D_3 z_e^{\Phi} + B_2 z_e^{\Psi}}{\gamma_{23}^{BD}} \right) \right] \\
& - B_3 Q_{32}^{\Phi,\Psi}(z_0,\omega) \left[\frac{\varepsilon_z}{2\gamma_{32}^{BD}} + \left(\frac{i\omega}{2\gamma_{32}^{BD} U} + \varepsilon_x \frac{D_2}{\gamma_{32}^{BD}} \right) \left(\varepsilon_z \frac{i\omega}{2\gamma_{32}^{BD} U} + \varepsilon_x z_0 - \varepsilon_x \frac{D_2 z_e^{\Phi} + B_3 z_e^{\Psi}}{\gamma_{32}^{BD}} \right) \right] \\
& + \left(B_1(z_0 - z_e^{\Phi}) - D_1(z_0 - z_e^{\Psi}) \right) Q_{11}^{\Phi,\Psi}(z_0,\omega) \left[\varepsilon_y z_0 + y_e^{\Psi} z_e^{\Phi} - y_e^{\Phi} z_e^{\Psi} \right] \\
& + B_3 Q_{31}^{\Phi,\Psi}(z_0,\omega) \left[\frac{i\omega}{2\gamma_{31}^{BD} U} + \varepsilon_x \frac{D_1}{\gamma_{31}^{BD}} \right] \left[\varepsilon_y z_0 + y_e^{\Psi} z_e^{\Phi} - y_e^{\Phi} z_e^{\Psi} \right] \\
& - D_3 Q_{13}^{\Phi,\Psi}(z_0,\omega) \left[\frac{i\omega}{2\gamma_{13}^{BD} U} - \varepsilon_x \frac{B_1}{\gamma_{13}^{BD}} \right] \left[\varepsilon_y z_0 + y_e^{\Psi} z_e^{\Phi} - y_e^{\Phi} z_e^{\Psi} \right].
\end{aligned}
\tag{65}
$$

To derive the result in Eq. (48) and above in Eq. (65) we needed to use the following integrals:

$$
\int_{-\infty}^{\infty} e^{i\omega t} e^{-\gamma_1 (t-\delta_1)^2} e^{-\gamma_2 (t-\delta_2)^2} = f_{\omega}(\gamma_1, \gamma_2, \delta_1, \delta_2),
$$

$$\int_{-\infty}^{\infty} te^{i\omega t}e^{-\gamma_1(t-\delta_1)^2}e^{-\gamma_2(t-\delta_2)^2} = \left[\frac{i\omega}{2\gamma_{12}} + \frac{\gamma_1\delta_1}{\gamma_{12}} + \frac{\gamma_2\delta_2}{\gamma_{12}}\right] f_\omega(\gamma_1,\gamma_2,\delta_1,\delta_2),$$

and

$$\int_{-\infty}^{\infty} t^2e^{i\omega t}e^{-\gamma_1(t-\delta_1)^2}e^{-\gamma_2(t-\delta_2)^2} = \left(\frac{1}{2\gamma_{12}} + \left[\frac{i\omega}{2\gamma_{12}} + \frac{\gamma_1\delta_1}{\gamma_{12}} + \frac{\gamma_2\delta_2}{\gamma_{12}}\right]^2\right) f_\omega(\gamma_1,\gamma_2,\delta_1,\delta_2),$$

where

$$f_\omega(\gamma_1,\gamma_2,\delta_1,\delta_2) = \sqrt{\frac{\pi}{\gamma_1+\gamma_2}}\exp\left(-\frac{\omega^2}{4(\gamma_1+\gamma_2)}\right)\exp\left(i\omega\left[\frac{\gamma_1\delta_1+\gamma_2\delta_2}{\gamma_1+\gamma_2}\right]\right)\exp\left(\frac{\gamma_1\gamma_2}{\gamma_1+\gamma_2}\left[2\delta_1\delta_2-\delta_1^2-\delta_2^2\right]\right).$$

B. Analytical calculation of integrals $I_\gamma^{1/2}$ and $I_\gamma^{3/2}$

The integrals are defined by

$$I_\gamma^{1/2}(z_0,\omega) = \int_0^\infty x_1^{1/2}e^{i\omega x_1/U}\exp[-\gamma\tan^2\alpha\,(x_1+\cos\alpha f(z_0)+\cot\alpha y_e)^2]\mathrm{d}x_1,$$

and

$$I_\gamma^{3/2}(z_0,\omega) = \int_0^\infty x_1^{3/2}e^{i\omega x_1/U}\exp[-\gamma\tan^2\alpha\,(x_1+\cos\alpha f(z_0)+\cot\alpha y_e)^2]\mathrm{d}x_1.$$

We further define the terms

$$\nu(z_0) = \cos\alpha f(z_0)+\cot\alpha y_e,\quad \mu(z_0,\omega) = \left(2\gamma\nu(z_0)\tan^2\alpha + \frac{i\omega}{U}\right)^2,\quad \lambda(z_0,\omega) = \frac{\mu(z_0,\omega)}{8\gamma\tan^2\alpha},$$

and then

$$I_\gamma^{1/2}(z_0,\omega) = \frac{\exp(-\gamma\nu^2\tan^2\alpha)\exp(\lambda)}{2\gamma^{1/2}\mu^{1/4}\tan\alpha}\left[2\lambda K_{5/4}(\lambda) - (1+2\lambda)K_{1/4}(\lambda)\right]\mathrm{sgn}(\nu(z_0)),$$

where we have suppressed the arguments of ν,μ and λ. We can also calculate that

$$I_\gamma^{3/2}(z_0,\omega) = \frac{\exp(-\gamma\nu^2\tan^2\alpha)\exp(\lambda)}{2\gamma^{1/2}\mu^{3/4}\tan\alpha}\left[2\lambda(1+4\lambda)K_{7/4}(\lambda) - \left(3+12\lambda+8\lambda^2\right)K_{1/4}(\lambda)\right]\mathrm{sgn}(\nu(z_0)).$$

Note that we implement $\mu^{1/4}$ as $\left(2\gamma\nu(z_0)\tan^2\alpha+i\omega/U\right)^{1/2}$ for sake of clarity, with the $\mu^{3/4}$ implemented as a power of 3/2. The sgn is there merely to ensure we take the correct root when we take that 4th root of μ, and is defined as

$$\mathrm{sgn}(x) = \begin{cases} -1 & x \le 0 \\ 1 & x > 0, \end{cases}$$

where we need $\mathrm{sgn}(0) = -1$ so we have agreement when the serration is in fact straight.

Acknowledgments

This work was supported by the UK Engineering and Physical Sciences Research Council (EPSRC) grant EP/H023348/1 for the University of Cambridge Centre for Doctoral Training, the Cambridge Centre for Analysis.

References

[1]Haeri, S., Kim, J., Narayanan, S., and Joseph, P., "3D calculations of aerofoil-turbulence interaction noise and the effect of wavy leading edges." *20th AIAA/CEAS Aeroacoustics Conference*, 2014.

[2]Narayanan, S., Joseph, P., Haeri, S., Kim, J., Chaitanya, P., and Polacsek, C., "Noise reduction studies from the leading edge of serrated flat plates," *20th AIAA/CEAS Aeroacoustics Conference*, 2014.

[3]Howe, M. S., "Aerodynamic noise of a serrated trailing edge," *Journal of Fluids and Structures*, Vol. 5, No. 1, 1991, pp. 33–45.

[4]Fish, F., "WhalePower Corporation," http://www.whalepowercorporation.com/, 2011.

[5]Howe, M. S., "Trailing edge noise at low Mach numbers," *Journal of Sound and Vibration*, Vol. 225, No. 2, 1999, pp. 211–238.

[6]Howe, M. S., *Acoustics of fluid-structure interactions*, Cambridge University Press, 1998.

[7]Duffy, D. G., *Green's functions with applications*, CRC Press, 2001.

[8]Lighthill, M. J., *An introduction to Fourier analysis and generalised functions*, Cambridge University Press, 1958.

[9]Wilson, D. K., "Turbulence models and the synthesis of random fields for acoustic wave propagation calculations," Tech. rep., DTIC Document, 1998.

[10]Howe, M. S., "Edge-source acoustic Greens function for an airfoil of arbitrary chord, with application to trailing-edge noise," *The Quarterly Journal of Mechanics and Applied Mathematics*, Vol. 54, No. 1, 2001, pp. 139–155.

[11]Ayton, L. J. and Peake, N., "On high-frequency noise scattering by aerofoils in flow," *Journal of Fluid Mechanics*, Vol. 734, 11 2013, pp. 144–182.